A PV Tied Single Core Triple Inductor Based Multi-Channel LED driver for Greenhouse Applications

Halleluyah Kupolati
Prof M.N. Gitau
University of Pretoria
njoroge.gitau@up.ac.za
hallkupolati@gmail.com

Centre for Renewable and Sustainable Energy Studies

Abstract
In the case of growth of plants in a greenhouse, there is a need for multi-channel LED drivers. This could be done using a pre-regulator followed by a linear current regulator using a MOSFET. However, this presents issues such as discontinuous current and potentially a discontinuous light intensity or a slight flicker observed by the LEDs. Hence, a continuous current is required for a more stable light intensity. An issue with parallel connected converters is the magnetic component count, i.e. the inductor count required leading to a space issue. In the quest to reduce the size of the system, a multi channel converter using a single toroid core is proposed. The system is programmed to source its power from a photovoltaic array. Hence, a requirement for the driver to act as a charge controller. This paper outlines the design and implementation system made up of a triple paralleled buck converter utilising a single ferrite core.

Keywords: Single Inductor Multiple Output(SIMO), Multiple Channel LED(MCLED), Pulse Width Modulation(PWM)

1. Introduction

An LED driver serves as a power supply for LED arrays. Additionally, it could be passive or active depending on the characteristics of the LED. Passive LED drivers make use of only passive components such as inductors, resistors and capacitors. An example of such a topology is implemented in (Ron Hui *et al.*, 2010; Lee, Nguyen and Rim, 2015). Often, the use of resistors is for the purpose of current limiting. The complexity of passive drivers tend to lag those of active drivers. However, considerations have to be made in its design to ensure that the voltage ratings of the connected LED array are not exceeded. Active drivers are typified by the use of at least one active component, such as a MOSFET, or an IGBT. The complexity of which can range from a linear current regulation system, (Park and Rim, 2013) to resonant converters, (Chen *et al.*, 2015). The operation of a typical LED follows the I-V curve. However, the current-voltage characteristics change as a result of a change in temperature, typically requiring a higher current to maintain the same intensity. Additionally, due to the need for active components, the system can potentially be designed to be more robust.

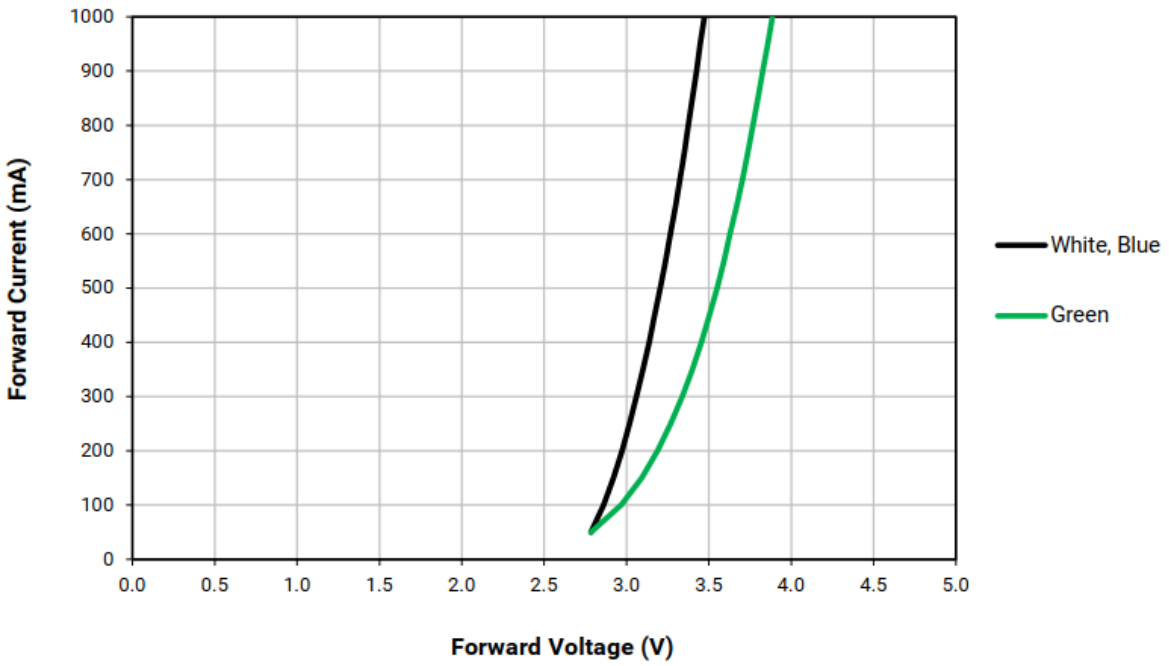

Figure 1 Current-Voltage Curve of an LED

In horticultural lighting applications, the use of mixed colour lighting has been found to be efficacious in the growth process of plants, (Izzo *et al.*, 2020; Shao *et al.*, 2022). These conclusions were made according to studies that monitored their effects on certain highlighted criteria such as dry weight, fresh weight etc. Different voltage-current requirements for LEDs necessitates the need of varying operating voltages for each LED array; the use of multi-channel LED(MCLED) drivers are required for such applications. Certain suggestions have been made on how to achieve multiple channel independent current control. A voltage pre regulator can be used followed by linear current regulators using MOSFETs to regulate the amount of current into each individual channel, (Hu *et al.*, 2019). Although this method presents an advantage in terms of its reduced cost associated with the low component count, it presents certain disadvantages as well. The switching frequencies required to operate the LEDs are on the lower end, i.e. approximately 4kHz, hence, the possible requirement for larger sized input LC filters.

On the other hand, continuous current MCLED drivers allow operation of the MOSFET devices at higher switching frequencies, approximately 50kHz and above. However, depending on the topologies used, these types of drivers tend to have an inductor, subsequently, requiring the need for a freewheeling diode. With the implementation of such systems, certain drawbacks become apparent, the principal of which are the number of the magnetic components required, i.e. each converter requires an inductor. Secondly, is the design of the control scheme, considering the effects of a constantly varying voltage input could result in a complex controller design. Due to the cost associated with a high component count, there is a need for the development of MCLED drivers that require a reduced number of components for full operation and functionality. Inductors that require ferrite cores are often the largest component in a power electronic device, hence, the most effective way of size reduction of the overall system is the reduction of the number of magnetic cores required to realise a MCLED driver.

DC-DC LED drivers require a DC source of electricity, which can either be a fixed voltage power supply, a photovoltaic(PV), or a battery. In the case of the use of PV panels as the power source for MCLED drivers, the driver has to act as a solar charge controller, (Zhang and Ma, 2015; Tran *et al.*, 2017). The charge controller could either operate in a fixed duty

cycle method referred to as PWM charge controllers or it could operate in MPPT mode. Extensive research done previously has shown that MPPT are more effective than PWM charge controllers in extracting the maximum power of a PV system. The core of the MPPT charge controller is the algorithm implemented. There exists three major basic types of algorithms, The fixed voltage method, the perturb and observe method, (Chellakhi, el Beid and Abouelmahjoub, 2022) and the incremental conductance, (Ahmed *et al.*, 2022) approach. There exists more advanced types of algorithms such as the particle swarm optimization(PSO) algorithm, (Baliyan, Jamil and Rizwan, 2021) and the estimate perturb perturb algorithm, (Kamran *et al.*, 2020).

1.1. The Multi-channel LED driver

As stated in the introduction, the purpose of the MCLED driver is to produce varied voltage levels for each channel. For the sake of clarity, the nature of the control of the output channels can be categorised into two groups, dependent and independent channel control. Dependent channel control indicates that the power level change of each channel has no effect on the other channels. On the opposite side, dependent channel control indicates that power level change of one channel affects the others.

In certain topologies, the control complexity of the independent is often higher than the dependent. An example of such a topology is a single inductor multiple output(SIMO) converter operating in DCM, (Kim *et al.*, 2014; Barwar *et al.*, 2020). On the other hand, the dependency on hardware precision tends to be higher in dependent channel control system.

An example of a system realising dependent channel control is a modified flyback topology, (Nagesha, Sreedevi and Gopal, 2015; Tahmaz and Yildiz, 2021) . A secondary side multiple winding transformer is used to realise the system. With such a system, precision is required in making the transformer so as to ensure that each channel produces the desired relative voltage level. It has been observed that a major requirement for MCLED driver systems having independent channel control is the presence of at least one MOSFET for each channel, (Huang *et al.*, 2011). In the control of these drivers, the control complexity could potentially increase as a result of the amount switching devices needed to realise them.

1.2. The Solar Charge Controller

The flow diagram below illustrates the flow diagram of a typical MPPT charge control algorithm, specifically the perturb and observe algorithm. In conventional DC-DC converters, the control output of the algorithm typically controls a single switching device, with the exception of a synchronous topology that requires multiple switching devices. In this application, multiple varied current setpoints exist. Hence, the duty change output of the MPPT algorithm will serve to increase or decrease multiple duty cycles. In order to mitigate control complexity, a hysteresis controller is used, which blends in with either the increase or decrease of a duty cycle implemented in the charge control algorithm.

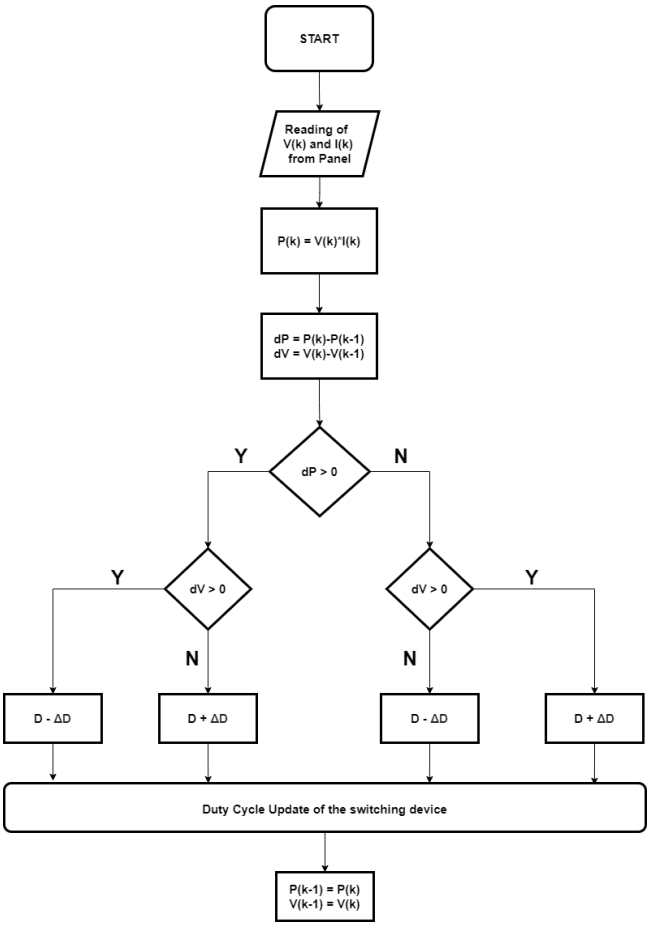

Figure 2 Flow diagram of perturb and oberve MPPT algortihm.

In hysteresis control, a setpoint is set. When the current goes beyond this point, the duty cycle is decreased. Likewise, when the current goes below this point the duty cycle is increased. The flow diagram represents a potential modification to the conventional MPPT algorithm for operation of the MCLED driver system. With regards to charge controller topologies, they have been realised using several topologies, (Hossain, Khan and Shafiullah, 2012; Baliwant, Gothane and Waghmare, 2019; Neethu and Senthilkumar, 2019)**.** It is noted that the use of some topologies such as the SEPIC or the cuk topology result in a high component count, i.e. two inductors required. For further increase in the efficiency of the system, synchronous topologies are often used.

1.3. Objectives

The aim of this work is to design and implement a PV tied MCLED driver system. The system is made up of 3 channels. The design will be aimed at achieving independent channel control. To achieve a reduction in the number of cores required, the inductors required by the three channels are wound on a single core.

Due to the nature of the inductors, there will be a focus on how much the independent channel control as well as the drain to source voltages of the MOSFET devices are affected by the mutual coupling of the inductors.

Hysteresis control scheme will be used to keep the output current of each channel constant. As a result of the control scheme being used, it is expected that the amount of power required by each channel is extracted from the PV array.

In section 2, the block diagram including the design and determination of the power components is outlined. In section 3, the research methodology is given in order to outline and clarify the approach to the research and the method in which the results will be

obtained and discussed. Subsequently, section 4 outlines the results obtained, additionally, the observations will be discussed. Lastly, the report is concluded in section 5 regarding the level of achievement of the primary objective and future recommendations are given.

2. Proposed model or Conceptual method

In this section, there will be an outline of the design and implementation of the multi-channel LED driver. Additionally, explanations will be given regarding the choice of the power and magnetic components used.

2.1. System Structure and General Operation

The block diagram shows the structure of the system. It comprises of the source, which in this case is a solar panel array operating at 18.8V, with an output range of 9V to 14V. The LED arrays used are rated for 50W. Hence, a maximum output current draw of 3.57A on each channel. Corresponding to the input, with the assumption of an 80% efficient converter, the average input current for each channel at that point in time can be obtained as (50/0.8)/(18.8) which amounts to 3.32A. An LC filter is implemented in order to prevent the draw of discontinuous current from the solar panel which could potentially cause unwanted heating of the panel connection cables. The first block is the switching and the diode freewheeling stage. The second block is made up of the three inductors all embedded on a single core.

The system is implemented in two parts. The first part is the implementation of an LC filter with linear current regulators using low side MOSFETs. The second part includes the freewheeling diode, and an output LC filter for each channel. The second part serves as a modifier for the first part in order to transform the output from a discontinuous current output to a continuous current output.

Additionally, the inductors required for the three output converters are placed on a single core.

Due to the system structure implemented, the current sensor is placed across the MOSFET. In the case of system operation in the first configuration, the load current through the LED array is obtained. However, during system operation in the second configuration, the input current of the buck converter is obtained. Due to the inductor operation in DCM, the relationship between the output current and the input current is not governed entirely by the duty ratio, hence, a difficulty in the determination of the output current using the input current.

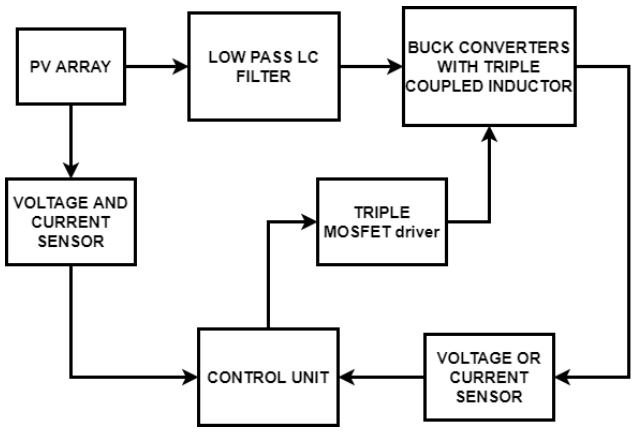

Figure 3 Proposed System Block Diagram

2.2. Buck Converter Design

In this section, the analysis of the operation of the buck converter is outlined. The power components are calculated according to the operation of a buck converter in DCM. The images below show the graphs associated with the operation of a buck converter in DCM.

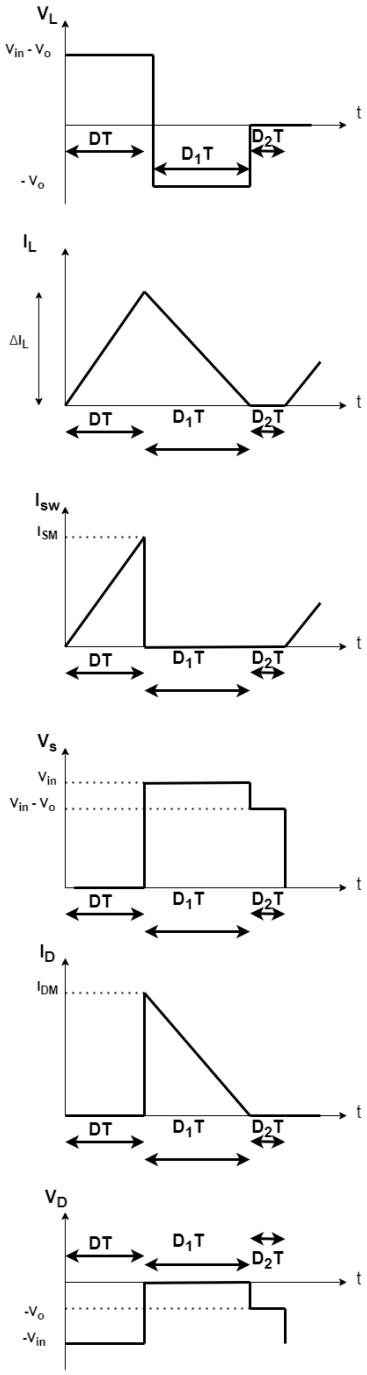

Figure 4 Voltage and Current waveforms for a Buck Converter in DCM.

The overall system circuit is indicated below

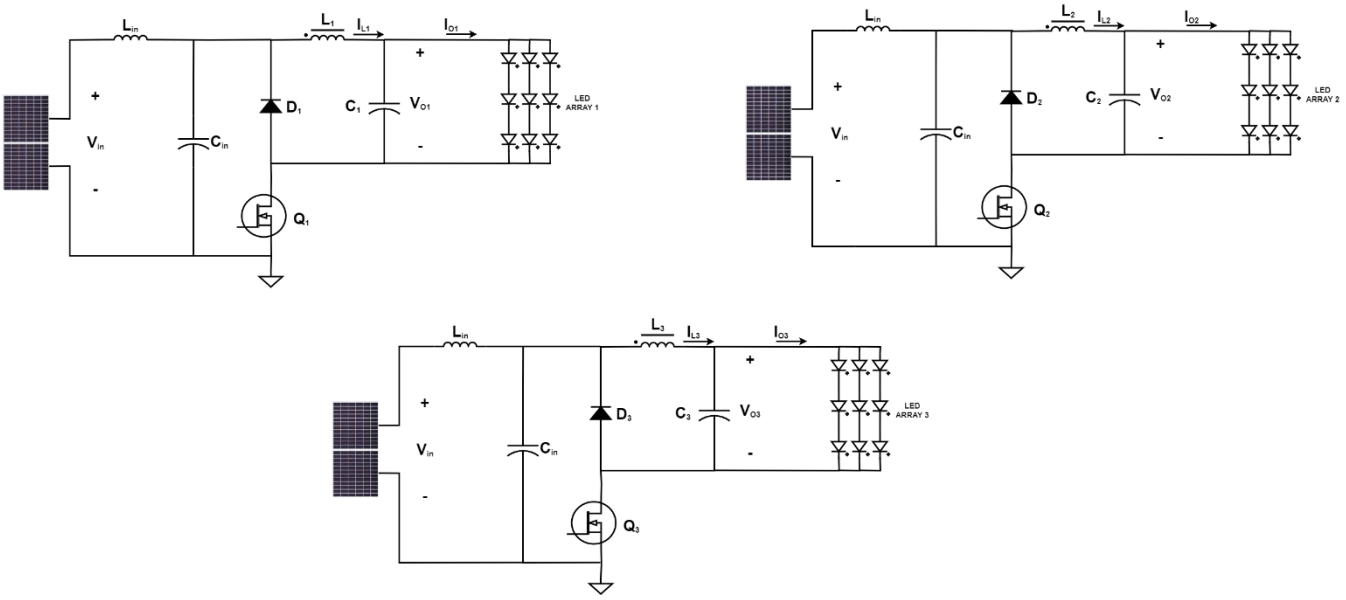

Figure 5 System Power Circuitry Schematic Indicating Coupling between the three Inductors.

Using the following parameters,

$$V_{in} = 18.8\,V,\ V_{out} = 9 - 14\,V,\ \Delta V_{o,pk-pk} = 0.02V_{o,ave},\ \Delta I_{L,pk-pk} = 2I_{L,ave},$$
$$I_{L,ave} = I_{out},\ V_{ce,sat} = 0.184V,\ V_{fwd} = 1.15V,\ r_L = 100m\Omega, I_{out} = 3.5A$$

The maximum duty cycle is calculated as follows

$$\delta_{max} = \frac{V_{fwd}+I_{L,ave}r_L+V_{out}}{V_{in}-V_{ce,sat}+V_{fwd}} = 0.784$$

The maximum allowable inductance is **calculated as follows**:

$$L_{max} = \frac{\left(V_{in}-V_{ce,sat}-I_{L,ave}r_L-V_{out}\right)\times\delta_{max}}{2I_{L,ave}f_{sw}} = 9.56\mu H$$

The capacitance required is calculated **using the following equation:**

$$C_{max} = \frac{2I_{L,ave}}{8\Delta V_{c,pk-pk}f_{sw}} = 62.5\mu F$$

The sizing of the power components is governed by the conduction mode, the disadvantage of which is the current stress on the switching devices.
Utilising a safety factor of 2 with the input and inductor peak currents, and the input and output voltage, an IRF8010 MOSFET and an apu3006 diode is chosen for this application. Additionally, with regards to the conventional PWM LED driver, the controller used is

2.3. Triple Coupled Inductor Design

The goal of the system is space reduction with the use of a single inductor core for the LED driving stage. A toroidal inductor is used to limit the possibility of a space-consuming snubber circuitry as a result of leakage inductance. With regards to toroidal inductors, a limit exists on the frequency that they can operate for the purpose of reduction of losses.

The motivation for the choice of operating frequency are for the limitation of the component sizes in addition to an adequate pwm resolution needed for the hysteresis control.

A 43 material core is used for the system, hence a limit on the operating frequency to be at 1MHz, at which point the core permeability begins to drop.

Taking into the account the available core area required by each inductor on the same core, the turns required is calculated as follows:

$$h = 15mm,\ r_o = 29.0mm,\ r_i = 19.0mm,\ \mu_o = 4\pi\times10^{-7},\ \mu_r = 800$$

$$N = \sqrt{\frac{0.6667\pi\times L}{h\times ln\left(\frac{r_o}{r_i}\right)\times\mu_o\mu_r}} = 1.77$$

Since the area available is larger than that required by the number of turns, the number of turns can be increased. To further achieve the objective of observing the effects of the mutual coupling on the drain to source voltages of the MOSFET devices, slight changes are made to the turns utilised for the coupled inductor. The number of turns utilised is 10 turns for the inductors on channel 1 and 2 and 8 turns for the inductor on channel 3.

2.4. Current Control

For realisation of the controller, five sensors are used. The solar panel output voltage and current sensor. Additionally, 3 sensors are used to determine the current of each channel. The system is designed to be transformable from a conventional PWM driver into a continuous current driver. Hence, the current sensor and protection fuse is placed in series with the MOSFET that serves as the linear current regulator for the in the conventional PWM driver configuration. Therefore, in the system configuration for continuous output current, the input current of the buck converter is being controlled. This current sensor placement has the advantage of protection of the switching from overcurrent.

The disadvantage is a need for a low pass filter current sensor in addition to a lack of current sensing on the output LED array. However, noting that the application demands only relative levels of current on each channel, it is deemed an acceptable compromise.

A hysteresis controller is used to realise current control.

The controller is implemented using a digital signal microprocessor. Specifically, the dsPIC33ev256gm102, operating at 140MHz, implementing a 12 bit ADC, and a 10 bit PWM resolution at 50kHz.

3. Research methodology

This section highlights the method used in the process of the research. Additionally, it includes the experimental setup and the steps used to obtain the results.
The data collected are the voltage and current readings at specific points of interest. Hence, the method for data collection is quantitative.

In summary, the major research steps are as follows:

- Research into the need for MCLED drivers, as well as their state of advancement.
- Select the suitable components for the design of the active and magnetic components of the circuit.
- Make observations on the performance of the system and discuss them.
- Conclude on how the level of achievement of the objectives and ways to move the research forward.

The following are the apparatus used for data collection:

- A Tektronix oscilloscope.
- AC/DC current probes.
- Voltage probes.
- Connecting wires.
- Three 50W LED array units, a separate LED array unit is required for each channel.
- The designed and implemented MCLED driver.
- A USB storage device to save the results.

The following steps are followed in order to obtain the experimental results:

- The coupling is set to DC for both the voltage and the current probe on the oscilloscope.
- The voltage is confirmed to have a scaling of 1 and the current probe is confirmed to have a scaling of 100mV/A.
- The required connections are made, i.e. the solar panel connection to the system and the connection of the conventional PWM driver to the second stage modifying system.
- The system is turned on and measurements are taken of the inductor current, the output voltage and current of the solar panel, as well as the LED array voltage and current for all channels.

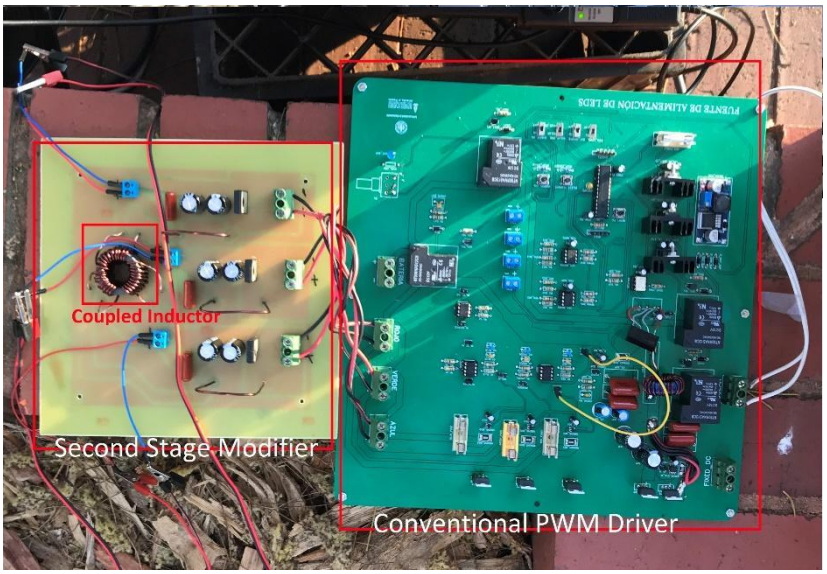

Figure 6 The realised MCLED driver

Figure 7 The Complete Experimental Setup

4. Results

This section outlines the results obtained from the system. The experiments aim to indicate independent channel control of MCLED drivers. The results below show the inductor waveform, and the output current of each channel. The duty cycle for each channel is shown. Subsequently, the output current for each channel is shown. Three LED arrays are connected to the overall system. One array on each channel.

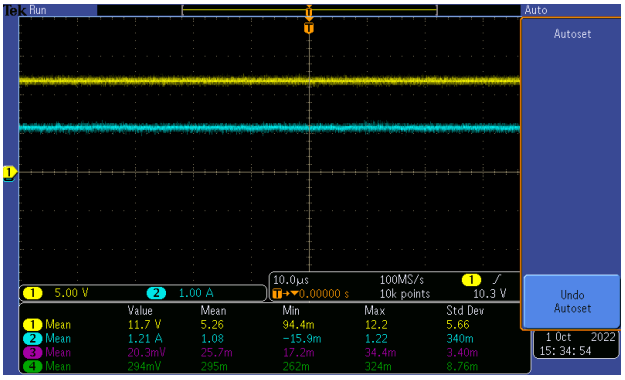

Figure 8 Input Voltage and Current of the PV panel. (5V/div, 1A/div)

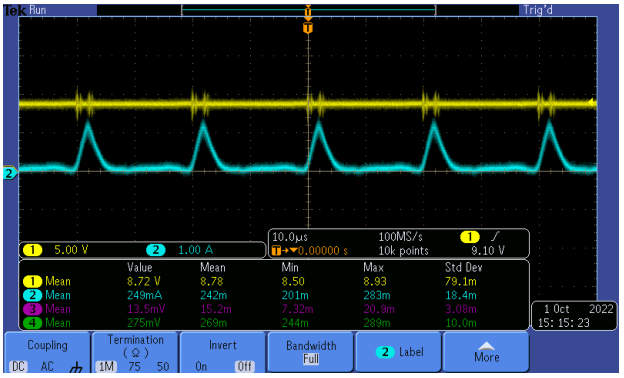

Figure 9 Output Voltage and Inductor Current of Channel 1.(5V/div, 1A/div)

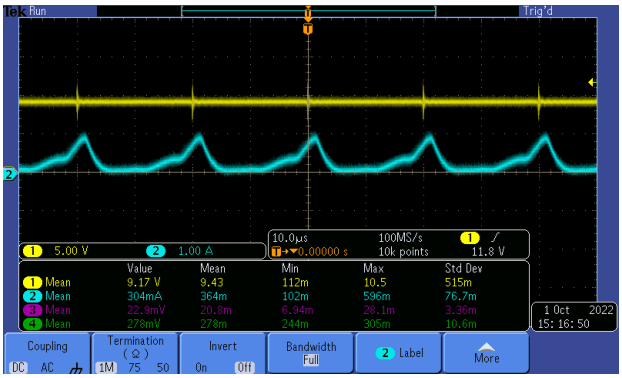

Figure 10 Output Voltage and Inductor Current of Channel 2.(5V/div, 1A/div)

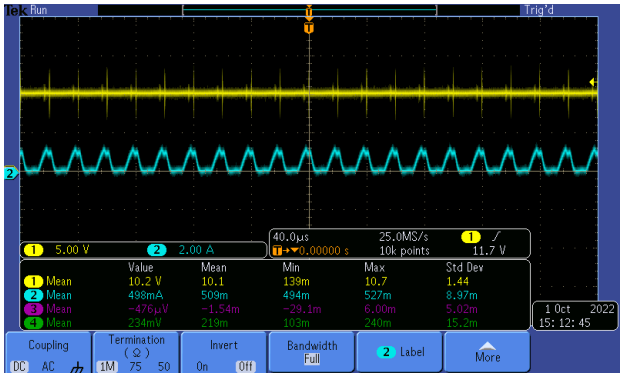

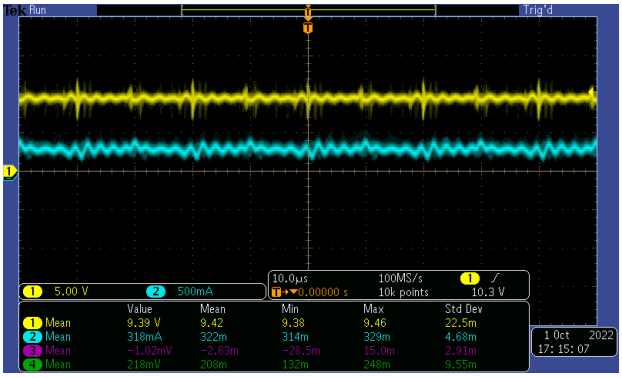

Figure 12 Output Voltage and Current of Channel 1(5V/div, 500mA/div)

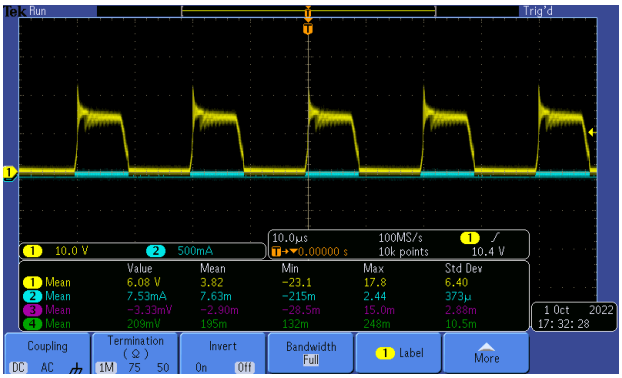

Figure 13 Drain to Source Voltage of MOSFET 1(10V/div)

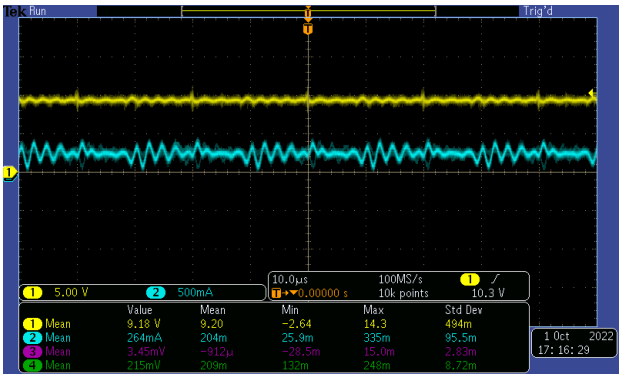

Figure 14 Output Voltage and Current of Channel 2(5V/div, 500mA/div)

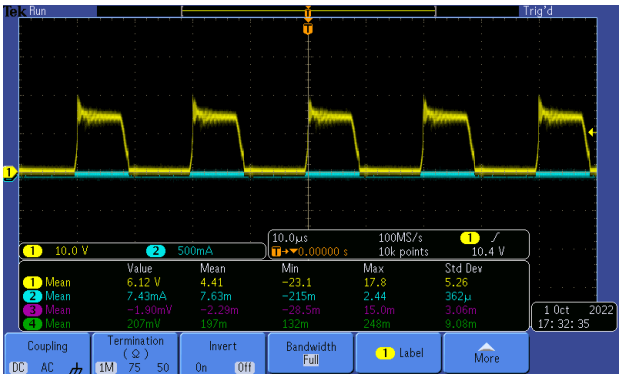

Figure 15 Drain to Source Voltage of MOSFET 2(10V/div)

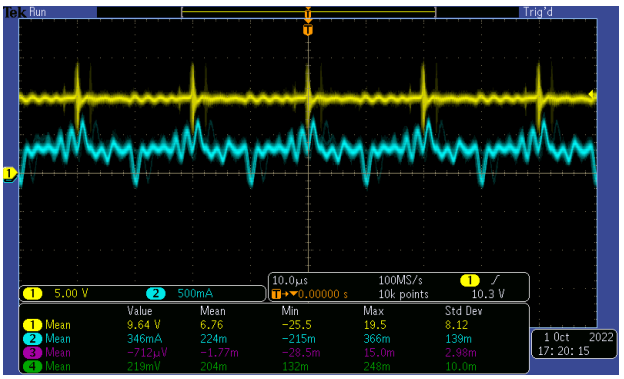

Figure 16 Output Voltage and Current of Channel 3.(5V/div, 500mA/div)

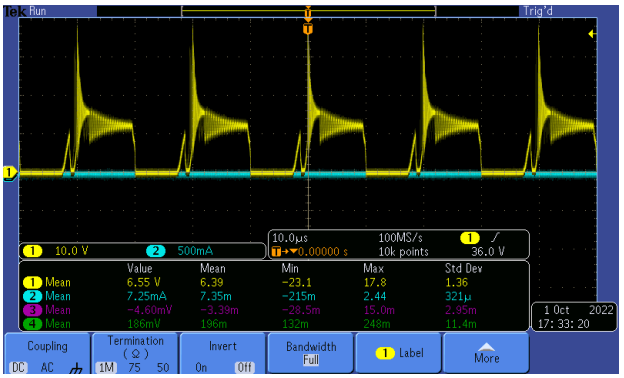

Figure 17 Drain to Source Voltage of MOSFET 3(10V/div)

The results indicate current waveform on each channel. As is evident, the current measured through each inductor is discontinuous following the designed routine. Due to the amount of turns used in the practical system exceeding that which was designed, the inductor might slip into a CCM mode of conduction as it gets closer the rated value.

The drain to source voltage of the channel 3 MOSFET exhibits a significantly larger spike than that of channels 1 and 2. Therefore, it appears that there exist significant levels of leakage inductance. This could be as a result of the lower number of turns present on channel 3 than the other channels. Additionally, the output voltage of the third channel had a tendency to be higher than the other channels at the same duty cycle.

With regards to the efficiency of the system, the results were taken in the later part of the afternoon with lower irradiance levels. Hence 15W was extracted from the 50W solar panel. The efficiency of the system at that voltage level was recorded to be 66.2%. It appears that the voltage spikes on the drain to source of the MOSFETs played a role in the relatively low efficiency. Additionally, operation of the system a certain amount below its rated value contributed to the low efficiency.

Regarding the stability of the waveform, the current sensor placement has an effect on that outcome. However, the current sensor placement increases the robustness of the system, in the sense that it is a transformable system from a conventional PWM driver into a continuous current driver.

In summary, the system implementing hysteresis current control is functional when connected to a PV panel. However, the system implemented appears to have a certain level of dependent current control across its channels. There is coupling between the inductors as a result of their placement on the same core. This causes the output voltages to be closer together with the exception of the case where there is a 0% duty cycle on one of the channels.

5. Conclusions and recommendations

The objective stated of the report was to obtain a PV tied MCLED driver with independent channel current control. Additionally, the driver was to be realised using three inductors on a single toroid core. The problem that was to be addressed was the size issue caused by connecting three buck converters in parallel. The SIMO buck converter topology was considered, however, the power capabilities to efficiency was deemed insufficient. The implementation of a triple coupled inductor resulted in a favourable outcome which led to the reduction in space required in comparison to the use of separate cores for each inductor. A compromise was made regarding the size of the inductor and the required size of the capacitor required for DCM applications. The system achieved the objective of being functional in receiving power from a PV source. The size issue was addressed because a multi channel converter was realised. However, independent channel control was not fully realised.

Recommendations for possible increase in efficiency of the SIMO converter is the use of an active snubber. With respect to the closed loop current control of the independent channels, the settling time can be decreased with the use of a higher order active low pass filter for the current sensing. Additionally, with the use of lower on-resistance MOSFETs, an increased frequency is possible, further reducing the size of the inductor. In order to mitigate the effects of coupling between the channels, time multiplexing techniques could be researched into in the future to potentially realise independent channel control.

References

[1] Ahmed, E.M. *et al.* (2022) 'Enhancement of MPPT controller in PV-BES system using incremental conductance along with hybrid crow-pattern search approach based ANFIS under different environmental conditions', *Sustainable Energy Technologies and Assessments*, 50, p. 101812. Available at: https://doi.org/10.1016/J.SETA.2021.101812.

[2] Baliwant, B.B., Gothane, A.R. and Waghmare, V.B. (2019) 'PWM based charge controller for renewable energy applications using sepic converter', *Proceedings of the 3rd International Conference on Computing Methodologies and Communication, ICCMC 2019*, pp. 1051–1054. Available at: https://doi.org/10.1109/ICCMC.2019.8819755.

[3] Baliyan, A., Jamil, M. and Rizwan, M. (2021) 'PSO based intelligent approach for battery charging scheduling integrated with solar photovoltaic systems', *2021 2nd International Conference for Emerging Technology, INCET 2021* [Preprint]. Available at: https://doi.org/10.1109/INCET51464.2021.9456232.

[4] Barwar, M.K. *et al.* (2020) 'Topological overview of single-inductor based multiple-output channel LED driver', *2020 1st International Conference on Power, Control and Computing Technologies, ICPC2T 2020*, pp. 122–127. Available at: https://doi.org/10.1109/ICPC2T48082.2020.9071435.

[5] Chellakhi, A., el Beid, S. and Abouelmahjoub, Y. (2022) 'An improved adaptable step-size P&O MPPT approach for standalone photovoltaic systems with battery station', *Simulation Modelling Practice and Theory*, 121, p. 102655. Available at: https://doi.org/10.1016/J.SIMPAT.2022.102655.

[6] Chen, X. *et al.* (2015) 'Multichannel LED Driver With CLL Resonant Converter', *IEEE Journal of Emerging and Selected Topics in Power Electronics*, 3(3), pp. 589–598. Available at: https://doi.org/10.1109/JESTPE.2015.2417219.

[7] Hossain, M.I., Khan, S.A. and Shafiullah, M. (2012) 'Power maximization of a photovoltaic system using automatic solar panel tracking along with boost converter and charge controller', *2012 7th International Conference on Electrical and Computer Engineering, ICECE 2012*, pp. 900–903. Available at: https://doi.org/10.1109/ICECE.2012.6471696.

[8] Hu, Y. *et al.* (2019) 'A new adaptive drive voltage approach for LED driver', *Conference Proceedings - IEEE Applied Power Electronics Conference and Exposition - APEC*, 2019-March, pp. 721–726. Available at: https://doi.org/10.1109/APEC.2019.8722013.

[9] Huang, Z. *et al.* (2011) 'A small-area low-mismatch multi-channel constant current LED driver', *2011 IEEE International Conference of Electron Devices and Solid-State Circuits, EDSSC 2011* [Preprint]. Available at: https://doi.org/10.1109/EDSSC.2011.6117624.

[10] Izzo, L.G. *et al.* (2020) 'The role of monochromatic red and blue light in tomato early photomorphogenesis and photosynthetic traits', *Environmental and Experimental Botany*, 179. Available at: https://doi.org/10.1016/j.envexpbot.2020.104195.

[11] Kamran, M. *et al.* (2020) 'Implementation of improved Perturb & Observe MPPT technique with confined search space for standalone photovoltaic system', *Journal of King Saud University - Engineering Sciences*, 32(7), pp. 432–441. Available at: https://doi.org/10.1016/J.JKSUES.2018.04.006.

[12] Kim, H.C. *et al.* (2014) 'An AC-powered, flicker-free, multi-channel LED driver with current-balancing SIMO buck topology for large area lighting applications', *Conference Proceedings - IEEE Applied Power Electronics Conference and Exposition - APEC*, pp. 3337–3341. Available at: https://doi.org/10.1109/APEC.2014.6803785.

[13] Lee, E.S., Nguyen, D.T. and Rim, C.T. (2015) 'A novel passive type LED driver for static LED power regulation by multi-stage switching circuits', *Conference Proceedings - IEEE Applied Power Electronics Conference and Exposition -*

APEC, 2015-May(May), pp. 900–905. Available at: https://doi.org/10.1109/APEC.2015.7104456.

[14] Nagesha, C., Sreedevi, A. and Gopal, M. (2015) 'Simulation and hardware implementation of 24 watt multiple output Flyback converter', *Proceedings of the 2015 IEEE International Conference on Power and Advanced Control Engineering, ICPACE 2015*, pp. 366–370. Available at: https://doi.org/10.1109/ICPACE.2015.7274974.

[15] Neethu, M. and Senthilkumar, R. (2019) 'Soft Computing Based MPPT Controller for Solar Powered Battery Charger under Partial Shading Conditions', *5th International Conference on Electrical Energy Systems, ICEES 2019* [Preprint]. Available at: https://doi.org/10.1109/ICEES.2019.8719314.

[16] Park, C. and Rim, C.T. (2013) 'Filter-free AC direct LED driver with unity power factor and low input current THD using binary segmented switched LED strings and linear current regulator', *Conference Proceedings - IEEE Applied Power Electronics Conference and Exposition - APEC*, pp. 870–874. Available at: https://doi.org/10.1109/APEC.2013.6520313.

[17] Ron Hui, S.Y. *et al.* (2010) 'A novel passive offline LED driver with long lifetime', *IEEE Transactions on Power Electronics*, 25(10), pp. 2665–2672. Available at: https://doi.org/10.1109/TPEL.2010.2048436.

[18] Shao, M. *et al.* (2022) 'Alternation of temporally overlapped red and blue light under continuous irradiation affected yield, antioxidant capacity and nutritional quality of purple-leaf lettuce', *Scientia Horticulturae*, 295. Available at: https://doi.org/10.1016/j.scienta.2021.110864.

[19] Tahmaz, O. and Yildiz, A.B. (2021) 'Analysis, Modeling, and Simulation of the Multiple Output Flyback Converter used in Various Motor Drive Applications', *Proceedings of 2021 21st International Symposium on Power Electronics, Ee 2021* [Preprint]. Available at: https://doi.org/10.1109/EE53374.2021.9628294.

[20] Tran, T.K. *et al.* (2017) 'Construct and control a PV-based independent public LED street lighting system with an efficient battery management system based on the power line communication', *2017 IEEE 2nd International Conference on Direct Current Microgrids, ICDCM 2017*, pp. 497–501. Available at: https://doi.org/10.1109/ICDCM.2017.8001092.

[21] Zhang, Y. and Ma, D. (2015) 'A single-stage solar-powered LED display driver using power channel time multiplexing technique', *IEEE Transactions on Power Electronics*, 30(7), pp. 3772–3780. Available at: https://doi.org/10.1109/TPEL.2014.2350484.